
Article:
Paterson, T.E., Beal, S.N., Santocildes-Romero, M.E. et al. (3 more authors) (2017) Selective laser melting–enabled electrospinning: Introducing complexity within electrospun membranes. Proceedings of the Institution of Mechanical Engineers, Part H: Journal of Engineering in Medicine, 231 (6). pp. 565-574. ISSN 0954-4119

https://doi.org/10.1177/0954411917690182

Selective Laser Melting-Enabled Electrospinning: Introducing Complexity within Electrospun Membranes

Thomas E. Paterson [1] , Selina N. Beal [1], Martin E. Santocildes-Romero [1], Alfred T. Sidambe[1], Paul V. Hatton [1] *, Ilida Ortega Asencio [1]**

*Corresponding author for biocompatibility determination.

**Corresponding author for microfabrication.

[1] Bioengineering and Health Technologies Group, The School of Clinical Dentistry, University of Sheffield, Sheffield S10 2TA, UK.

Abstract

Additive manufacturing technologies enable the creation of very precise and well-defined structures that can mimic hierarchical features of natural tissues. In this paper we describe the development of a manufacturing technology platform to produce innovative biodegradable membranes that are enhanced with controlled microenvironments produced via a combination of selective laser melting techniques and conventional electrospinning. This work underpins the manufacture of a new generation of biomaterial devices that have significant potential for use as both basic research tools and components of therapeutic implants. The membranes were successfully manufactured and a total of 3 microenvironment designs (niches) were chosen for thorough characterisation. Scanning electron microscopy analysis demonstrated differences in fibre diameters within different areas of the niche structures as well as differences in fibre density. We also showed the potential of using the microfabricated membranes for supporting mesenchymal stromal cell (MSC) culture and proliferation. We demonstrated that MSCs grow and populate the membranes penetrating within the niche-like structures. These findings demonstrate the creation of a very versatile tool that can be used in a variety of tissue regeneration applications including bone healing.

Keywords

Additive Manufacturing, Selective laser melting, Electrospinning, Stem Cell Niche, Bone Healing

Introduction

During the past decade there has been a marked growth in the use of additive manufacturing technologies (AM) for medical and dental applications. AM offers great possibilities in terms of product development, control and prototype design from which the medical industry can definitely benefit [1-3]. Apart from a custom design, AM also provides

clear advantages including the opportunity for developing internal complexity, a significant reduction in waste materials and great possibilities for scaling-up [4].

Selective laser sintering (SLS), Stereolithography (SLA) and Fused Deposition Modeling (FDM) are three of the most commonly used techniques for the manufacture of scaffolds and biomaterial devices for regenerative medicine [1]. Although they are all based in the same principle, “layer by layer manufacturing”, the fundamental science behind each technique is very different and is intimately related to the availability of materials that can be structured and ultimately transformed into a medical device. Thus, in general terms, we could say that stereolithography and related techniques (including two-photon polymerisation) require the presence of a photocurable working solution [5, 6], selective laser sintering requires a material in a powder form [7, 8], and fused deposition modelling relies on working materials that can be extruded via temperature control [9, 10]. The possibilities offered by these techniques themselves are vast, although their potential can be enhanced further when combined with conventional techniques historically used for biomedical applications (e.g. electrospinning). Electrospinning is a versatile fabrication process that uses a high voltage between a syringe containing a polymer solution and an earthed collector in order to create 3D fibrous constructs. Controlling the processing conditions and the design of the collector is possible to manufacture complex membranes with different fibre alignment, diameter, porosity, and topography. The incorporation of additive manufactured collectors within the electrospinning process permits the creation of intricate structures with micron accuracy. This combination of techniques was patented in 2013 [11] and it was initially developed using microstereolithography for emulating aspects of the limbal stem cell niche in the cornea [12-14]. In essence, the continuous deposition of electrospun fibres on top of a 3D collector fabricated using additive manufacturing will result in the generation of mats that reproduce the underlying topography of the 3D collector. This way it is possible to provide the scaffold with levels of complexity that the electrospun fibres on their own cannot achieve.

There is an increasing interest in designing biomedical devices with the ability of directing cell behaviour via the inclusion of controlled and intricate topography. In the past 5 to 10 years, the design and fabrication of scaffolds containing well-defined microfeatures has been identified as a rapidly evolving field, and this growing body of research has shown that topography can be controlled using a wide range of fabrication routes including laser-based techniques [15-18], micromoulding [19, 20], compression-based techniques [21, 22] and electrospinning [12-14]. One powerful approach to create intricate topographies is the development of ‘synthetic niches’ that are designed to mimic specific aspects of the stem cell native niche. Stem cell niches can be described as complex and well-defined microenvironments that play a fundamental role in tissue repair, controlling to a certain extent stem cell renewal and differentiation [23]. The ability to recapitulate aspects of the stem cell microenvironment opens the door to a broad range of applications in regenerative medicine, especially in the design of smart biomaterial devices for tissue healing [24, 25]. There is a need to develop innovative biomaterial devices able to be delivered to the patient in conditions that mimic the physiological environment as closely as possible. The inclusion of the concept of “Stem Cell Niche” within their design philosophy would be an innovative and valuable approach in which additive manufacturing technologies play a key role, allowing the creation of custom devices presenting tailored features with dimensions in the scale of microns.

In this study, electrospinning has been combined with selective laser melting (SLM) to produce complex scaffolds in which to study and control cell behaviour. The use of SLM offers specific advantages. Firstly, the manufactured SLM-metallic collectors can be reused indefinitely, due to their durability, which can have a tremendous impact in the price of future

medical devices. Secondly, SLM offers great accuracy and it is already used in a variety of medical and dental applications [26]. Finally, the commercially available rig we have used allows the fabrication of between 10-15 collectors at once, making the process very efficient. We describe here the manufacture of a range of electrospun membranes incorporating different morphologies and distributions of synthetic microenvironments setting the basis for the design and future delivery of a new generation of devices with enhanced regenerative capability to be used in bone healing applications. These prototype membranes have been evaluated using mesenchymal stromal cells (MSCs) to determine biocompatibility and potential for control of stem cell populations.

Materials and Methods

1. Scaffold Fabrication and Characterisation

1.1. Manufacturing of SLM Collectors

The microfabricated electrospinning collectors were manufactured using a Renishaw SLM 125 machine and Stainless steel 316L. The plates were manufactured using a range of niche-like morphologies designed using CAD software (Solidworks). The specific processing parameters for the fabrication of the collectors were: Laser power 200W, Speed 480 mm/s, Point distance 50 micrometres, and exposure time 70 microseconds. The metallic collectors were then used as targets in a conventional electrospinning set-up for creating electrospun positive imprints (see Figure1).

1.2. Manufacturing of Microfabricated Electrospun Membranes

Electrospun membranes were fabricated using solutions of 10 wt% poly(caprolactone) (PCL) (Average Mw 80000; Sigma Aldrich, UK) prepared in a blend of dichloromethane (DCM) (Fisher Scientific, UK) and dimethylformamide (DMF) (Fisher Scientific, UK) with ratio 90/10 wt% DCM/DMF [27]. For this, PCL was added to the solvents and continuously stirred at room temperature until the polymer dissolved completely. Electrospinning was performed using equipment composed of a PHD2000 infuse/withdraw syringe pump (Harvard Apparatus, UK) and an Alpha IV Brandenburg power source (Brandenburg, UK). Plastic syringes (1 mL; Becton Dickinson, UK) were used to drive the solutions into 20-gauge blunt metallic needles (Intertronics, UK). The voltage applied was 17 kV, the flow rate was 2.5 mL/h, and the distance from the tip of the needle to the collector was 21 cm.

1.3. Characterisation of Electrospun Membranes

The topography of the SLM-fabricated collectors was studied using optical microscopy. The morphology and size of the synthetic electrospun niches was studied in greater detail using scanning electron microscopy (SEM, Philips X-L 20). Fibre diameter was measured inside and outside the niche-like areas using ImageJ software and SEM micrographs at a magnification of x800. Two (2) different samples were analysed and a total of 4 random areas per sample were examined. A final number of 80 fibres were measured for each of the cases.

For collecting micro-CT data, electrospun membranes were mounted in plastic straws (0.4 cm in diameter) and placed into the micro-CT machine (SKYSCAN 1272). No filter was used and pixel size was set at 4.5 µm with a 0.7° rotation step. No averaging was used and a 360° scan rotation was carried out. NRecon software was utilised to construct the image series using the following settings: 20% beam hardening, 2 smoothing setting, 4 ring artefact setting and 0 – 0.1 greyscale range was applied. An area of interest was chosen manually to contain several niche-areas, and then these specific areas were narrowed down.

2. Biological Testing

2.1. Culture of Mesenchymal Stromal Cell

Mesenchymal stromal cells (MSCs) were isolated from the bone marrow of 5-6 weeks old male Wistar rats following the method described by Maniatopoulos et al. [28]. The femora of 3 animals were dissected in aseptic conditions, cleaned of soft tissues, and immersed in 10 mL of Dulbecco's modified Eagle's medium (DMEM) (Sigma Aldrich, UK) supplemented with 100 units/ml of penicillin (Sigma Aldrich, UK) and 1 mg/ml of streptomycin (Sigma Aldrich, UK). The ends of the femora were removed and the bone marrows were flushed into 5 mL of DMEM supplemented with 10 units/ml of penicillin, 0.1 mg/ml streptomycin, 20 mM alanyl-glutamine (Sigma Aldrich, UK), and 10% v/v foetal calf serum (Biosera, UK). The cells were then seeded into 75 cm^2 culture flasks containing 10 ml of cell culture medium, and were incubated at 37℃ and 5% CO2 for 24 h. The non-adherent cells and debris were then washed away with fresh cell culture medium. All cell cultures were inspected daily and the medium was changed every 48 to 72 h. At near confluence, the adherent cells were removed from culture using 0.05% Trypsin/0.02% ethylenediaminetetraacetic acid (Sigma Aldrich, UK), pooled into a single population, and seeded for experimentation or stored for later use.
For cell culture purposes the electrospun microfabricated membranes were cut into circles/disks (13 mm diameter) and placed in 24 well plates. Test groups used were microfabricated scaffold with cells, plain sheet of electrospun PCL with cells, electrospun scaffolds without cells and TCP controls, 5 replicates and n = 3. The individual membranes were sterilised in 70% methanol and 30% dH_2O for 30 minutes before rinsing with PBS three times. Membranes were finally left submerged in 1 ml of media for 30 minutes before cells were added.

2.2. Metabolic Activity and Cell Morphology

The metabolic activity of cells on the 3 different niche designs and plain membranes (without added topography) was measured using PrestoBlue (resazurin-based dye, n=3). Cells were seeded at a concentration of 50,000 cells per scaffold, and fluorescence measurements were taken at 1, 7 and 14 days. Cell viability and proliferation in the microfabricated scaffolds was compared to both 2D-TCP (tissue culture plastic) controls and plain sheets of PCL electrospun scaffolds (membranes without microfeatures presenting randomly distributed fibres).

At each time point membranes were moved to a new well plate to prevent contamination of Prestoblue with any cells growing in the well. Cells were gently washed with PBS and the PrestoBlue reagent was mixed at a 1:9 ration in media and 700 µl added to each well for 90 minutes. Three aliquots of 200 µl were taken from each sample and fluorescence measurements were taken using a microplate fluorescence reader FLx 800 Bio-Tek Instruments using an excitation wavelength of 540 nm and an emission wavelength of 635 nm. After fluorescence measurements the PrestoBlue solution was removed, the cells were washed with PBS, fresh media was added and they were returned to the incubator.

For fluorescent staining, MSCs were seeded onto the electrospun membranes at a concentration of 20000 cells per scaffold and stained with Phalloidin-FITC (to label actin filaments) and DAPI (nucleic acid stain). At day 5 after cell seeding, the membranes were fixed in 3.7% formaldehyde in PBS for 20 min at room temperature. 0.1% of triton-X100 in PBS was added to the samples for 20 minutes before rinsing with PBS. Phalloidin-FITC

(1:500) and DAPI (1:1000) was added in PBS for 30 min. Cells were observed using a confocal scanning microscope (Carl Zeiss LSM510-META, Germany). Images (1024 x 1024 pixels) were obtained using a Zeiss LSM 510Meta inverted confocal microscope and x10/0.3 water dipping objective, with a pixel dwell time of 6.4 µs. Phalloidin-FITC was excited using a 488 nm laser (20% transmission) and emission detected 505 nm. DAPI was excited using an 800 nm laser (12% transmission) and emission detected between 435 and 485 nm. All image analysis was performed using Zeiss LSM image browser and ImageJ.

2.3. Histology

PCL scaffolds were mounted in tissue freezing medium (Leica) by submersion in liquid nitrogen. Samples were sectioned to 10 µm thickness using a cryostat (Leica CM1860 UV) at a controlled temperature of -24 ℃. Slides were rinsed gently under tap water to remove remaining cryostat Optimal cutting temperature (OCT) compound, and then, they were submerged on a rack in haematoxylin for 60 seconds before being rinsing with a constant flow of tap water for 5 minutes. Slides were then submerged in Eosin for 5 minutes and then 1 minute in water. Samples were exposed briefly to 70% Industrial Methylated Spirits (IMS), 95% IMS, and left for 30 seconds submerged in 100% IMS to dehydrate the sample. Samples were finally submerged in xylene before mounting under a coverslip.

2.4. Collagen deposition (Sirius red staining)

Scaffolds were washed in PBS 3 times and fixed in 3.7% formaldehyde. The scaffolds were then stained using a solution of 0.1% Sirius red in picric acid (Direct Red 80, C.I. 35780, Sigma-Aldrich) and placed on a rocker for 18 hours. The scaffolds were then washed with water until no further dye was eluted. For quantitative analysis scaffolds were de-stained in 1 ml of 0.2 M solution of NaOH and methanol (1:1) for 60 minutes on a rocker. Afterwards, 300 µl from each sample were added in triplicate to a 96 well plate and absorbance was measured at a wavelength of 490 nm using a spectrophotometer plate reader.

2.5. Stem Cell Markers

Samples were washed in PBS and then they were submerged in 0.1% formaldehyde for 15 minutes. CD44 antibody (Anti-rat with fluorochrome Alexa Fluor 647) (1:250) and DAPI (1:500) in PBS were added to the scaffolds for 1 hour before being washed with PBS. Images (1024 x 1024 pixels) were obtained using a Zeiss LSM 510Meta inverted confocal microscope and x10/0.3 water dipping objective, with a pixel dwell time of 6.4 µs. DAPI was excited using an 780 nm laser (8.1% transmission) and emission detected between 435 and 485 nm. CD44 was excited using a 633 nm laser (51% transmission) and emission detected between 650 and 710 nm. All image analyses were performed using Zeiss LSM image browser and ImageJ.

2.6. SEM fixation

Samples were washed with distilled water for 5 minutes then sequentially submerged in the following solutions of ethanol (prepared in distilled water) for 15 minutes each: 35%, 60%, 80%, 90% and 100%. Hexamethyldisilazane (HDMS) (Sigma-Aldrich) was made up to a 1:1 mixture with ethanol by weight and added to the samples for 1 hour. 100% HDMS solution was then added to submerge the samples for 5 minutes, twice. Samples were left to air dry and then gold coated.

3. Statistical Analyses

Statistical analyses were performed on GraphPad Prism software using two-tailed Student T-test, one-way ANOVA, and post-hoc Tukey tests. In all cases, p values <0.05 were considered as statistically significant.

Results

1. Niche and fibre diameter in the microfabricated electrospun mats

SLM allowed the creation of 3 cm x 7 cm rectangular collectors with 1 mm in thickness. The average niche diameter of the SLM collectors was calculated using optical micrographs and ImageJ (n=5). The average dimensions were 667 µm ± 85 (Niche1), 1038 µm ± 60 (Niche 2) and 1168 µm ± 170 (Niche 3). The electrospun replicas were analysed in the same way showing the following niche diameters: 892 µm ± 76 (Niche 1), 1158 µm ± 32 (Niche 2) and 1287 µm ± 134 (Niche 3) (See Figure 2 for optical microscopy and SEM images).

One-way ANOVA reported statistically significant differences ($F(8, 1071) = 3.937$, $p = 0.0001$) between the diameters of fibres belonging to electrospun mats with and without niches (see table 1 for the average values of fibre diameters). More specifically, post-hoc Tukey test showed that statistically significant differences between fibre diameters were found at niche locations 2a and 2b ($p < 0.05$), 2a and 3a ($p<0.0005$), and between the diameter plain mat (without niches) and location 3a ($p <0.005$) (see schematic of locations in Figure 3).

It was observed in the SEM images that the density of the fibres per mm^2 was visibly lower in the inner areas of the niche structures (see Figure 2 N-P). This was then corroborated with Micro-CT scans.

2. Rat MSCs characterisation on microfabricated electrospun mats

Rat MSCs grew and proliferated in the microfabricated scaffolds. MSCs were observed fully infiltrating the artificial stem cell niches, and confocal z-stacks enabled the accurate imaging of 3D niche areas (see Figure 4B). Sectioned samples showed cells did not penetrate greater than 40µm into the fibrous plain mats but they did achieve deeper penetration in niche areas, as mapped using the DephCod tool in the LSM Confocal software (See Figures 4E and 4F). SEM images corroborated cell attachment (See Figure 4D) and cell distribution showing that the cellular population of the niches was less dense than in the surrounding not microfabricated areas (See Figures 4C, 4D).

Discussion

Here we present for the first time the use of selective laser melting for introducing complexity within electrospun membranes for biomedical applications. The use of SLM for creating electrospinning collectors is versatile and efficient, as the designs can be easily changed and adjusted with a high degree of accuracy in terms of size, morphology, depth and distribution of the incorporated microfeatures. On the other hand, the metallic collectors can be re-used indefinitely (which is highly desirable from a future end-product point of view). Electrospun membranes are well-known due to their great potential as regenerative medicine constructs since they can mimic, to a certain extent, the 3D extracellular matrix, providing cells with mechanical support and with a porous environment in which to proliferate. In this work we have achieved the incorporation of a second level of complexity within our electrospun membranes, which has been introduced via the use of SLM. We have provided the electrospun constructs with artificial well-defined microenvironments as an extra tool for influencing cell behaviour. The development of niche-like environments is

indeed a new and rapid growing area of research [12-17, 19, 20, 29, 30]. In this specific study we have used SLM to aid in the development of electrospun membranes containing microfeatures and we have chosen 3 types of topography (niche structures) to develop a preliminary study using primary mesenchymal rat stem cells.

The accuracy in reproducing the features incorporated within the underlying metallic template was high (higher than 70% for the 3 topographies studied); it was observed that a decrease in accuracy of reproduction was intimately related with a decrease in the size of the microfeature. However, this fact does not present a problem for the proposed approach since we aim to work with features with dimensions ranging from 250µm to 1000µm, which are biologically relevant in terms of reproducing aspects of a physiological niche environment. It is also possible to accommodate for this effect when designing the templates, making the features a different size so that the eventual microfeatures on the electrospun material are the desired size and dimensions.

Fibre diameter was studied in different parts of the microenvironments (see schematic in Figure 3) and it was compared to a plain random mat of electrospun fibres. It was observed that the diameters corresponding to the areas in which the scaffold stretches to reproduce the morphology of the underlying collector the fibres presented a certain degree of alignment and, for these cases, the diameter was significantly smaller. These differences are consistent for all the distinct fibre patterns showed in this study and we attribute the changes in diameter to the stretching of the fibres during the formation of the scaffold. For example, for Niche 2, the bottom of the niche (a) presents a random distribution of fibres with a very similar diameter to the areas outside the niche (c); on the other hand, when we compare the diameter of the fibres in the bottom of the niche with the diameter on the wall of the niche (b) we observe a difference in the overall distribution of the fibres (which appear to be more aligned) and we also observe a significant difference in their diameter. Changes in fibre diameter can affect cell behaviour, as previously reported in the literature [31, 32]; in our case, we have performed an accurate study showing that our new methodology allow us to introduce complexity within the membranes creating niches with different fibre densities and different areas of fibre diameter which we hypothesise will have a direct effect in influencing cell behaviour.

Mesenchymal stromal cells were found to attach to our structures and they were located within the microfeatures (See Figure 4). Confocal Z-stacks provided us with information regarding the distribution of cells within the niche structures and in their surroundings as well as regarding the degree of cell penetration within the scaffolds. Cells were homogeneously distributed within the scaffolds and the use of heat maps was key in allowing us to visualise the areas in which cells populated the niche structures. Cells were able to proliferate on the PCL scaffolds as expected; (see PrestoBlue results in Figure 4). Proliferation rate was found to be slower for the cells seeded on the PCL electrospun mats compared to our Tissue Culture Plastic (TCP) controls; we anticipated this outcome, since differences in cell proliferation within 2D (tissue culture plate) and 3D (scaffolds) samples are well documented in the literature [33]. No significant differences were observed between the different types of scaffolds with niche morphologies 1-3 or when comparing the scaffolds to a plain mat of fibres; the inclusion of intricate topography does not seem to have a direct effect in the degree of cell proliferation which is supported by our previous publications in which comparable results were reported using equivalent metabolic activity assays [13, 14].

The cells were found to produce collagen, which was measured using Sirius Red (Figure 5), and no differences between a plain scaffold and the niche-decorated scaffolds were observed. Collagen production can be used as a guide to determine whether MSC cells

have differentiated into ECM producing cells such as Osteoblasts. The presence of extracellular collagen can indicate the proportion of cells present that are producing ECM, as an indicator of osteoblast activity. MSC cells have a rapid proliferation rate and produce lower quantities of ECM as a result. In contrast, the main function of an osteoblast cell is to produce ECM and to facilitate the calcification of bone. Further research needs to be carried out to determine the relationship between the niche-structures and osteoblastic behaviour, in this preliminary work we just aimed to demonstrate the general osteoblastic capability of our system.

In this study, CD44 was successfully imaged on the surface of MSCs using confocal microscopy; CD44 is a surface glycoprotein which is involved in cell adhesion, proliferation, differentiation and migration processes, and has also been associated with cancer stem cells [34]. The International Society of Cell Therapy (ISCT) has stated that positively identified human MSCs must express CD105, CD73 and CD90 [35]. However, the situation for animal models (a rat model in our case) is not as well defined; for example, CD105, CD73 and CD90 are not expressed equally by all species [36] and, on the other hand, additional markers, (such as CD44) are more consistently expressed across species. Nevertheless, the simultaneous presence of CD44 in many cell types (e.g. MSCs, haematopoietic stem cells, lymphoid, myeloid, megakaryotic, erythroid and endothelial cellular lineages) reduces its specificity and limits its use severely [36]. Additionally, evidence has shown that the levels of CD44 expression in rat bone marrow MSCs may vary significantly depending on animal strain and passage [37]. In this context, Barzilay et al [37] reported significantly high and constant levels of expression of CD90 and CD29 antigens on bone marrow MSCs isolated from four different rat strains and (at passages 2 and 7) which indicates that CD90 and CD29 would be a good alternative for a more extended study. In our preliminary study the number of CD44 positive cells seemed to be lower within the niche areas but exhaustive cell count studies need to be performed to support this claim and, as explained above, the use of extra markers will be necessary to fully understand the relationship between the niche environment and the specific behaviour of both a single cell and a cell population. Future work will focus on the use of CD90 and CD29 in order to enhance the identification of our MSC cells and determine if cell stemness is directly influenced by the presence of the microfabricated niche. In this sense, is also known that the incorporation of biomolecules and/or polymer coatings can also influence and direct cell behaviour [17, 38, 39]; current work developed in our laboratory is now focussing on the incorporation of specific biomolecules within our SLM-assisted optimised niche environments; these molecules are aimed to encourage stemness and we believe will be crucial in dictating the future regenerative capacity of the overall constructs.

To summarize, in this piece work we have successfully developed and established a manufacturing method for the fabrication of complex electrospun scaffolds containing niche-like structures and we have demonstrated the ability of these scaffolds to support MSC growth and proliferation showing the potential for these membranes to be used in bone regeneration and related musculoskeletal applications.

Conclusion

This paper reports for the first time a manufacturing method to rapidly and reproducibly fabricate intricate 3D features within biocompatible electrospun membranes using a metal template itself produced using SLM. These complex electrospun membranes have the potential to be used as tissue engineering scaffolds and/or as components of biomaterial devices with enhanced regenerative capability. The inclusion of SLM within the fabrication

process allows a wide range of possibilities of design and the creation of bespoke tailored features. Moreover, the metallic collectors used for electrospinning may be reused, so having a direct impact in future scaling-up procedures and commercialisation of the end product.

Acknowledgements

The authors would like to acknowledge the Women Academic Returners' Programme (WARP) at Sheffield for funding part of this work and MeDe Innovation (the UK EPSRC Centre for Innovative Manufacturing in Medical Devices, grant number EP/K029592/1).

Table Captions

Table 1. Average fibre diameters for each area of the Niche structures. Mean ± SD is presented in this table.

Scaffold site	Average fibre diameter (µM)	Standard deviation
Plain	2.2	0.8
Niche 1 a	1.9	1.6
Niche 1 b	2.0	1.1
Niche 1 c	2.0	1.0
Niche 2 a	2.2	1.1
Niche 2 b	1.8	0.9
Niche 2 c	2.0	0.9
Niche 3 a	1.7	0.8
Niche 3 c	1.8	1.0

Figure Captions

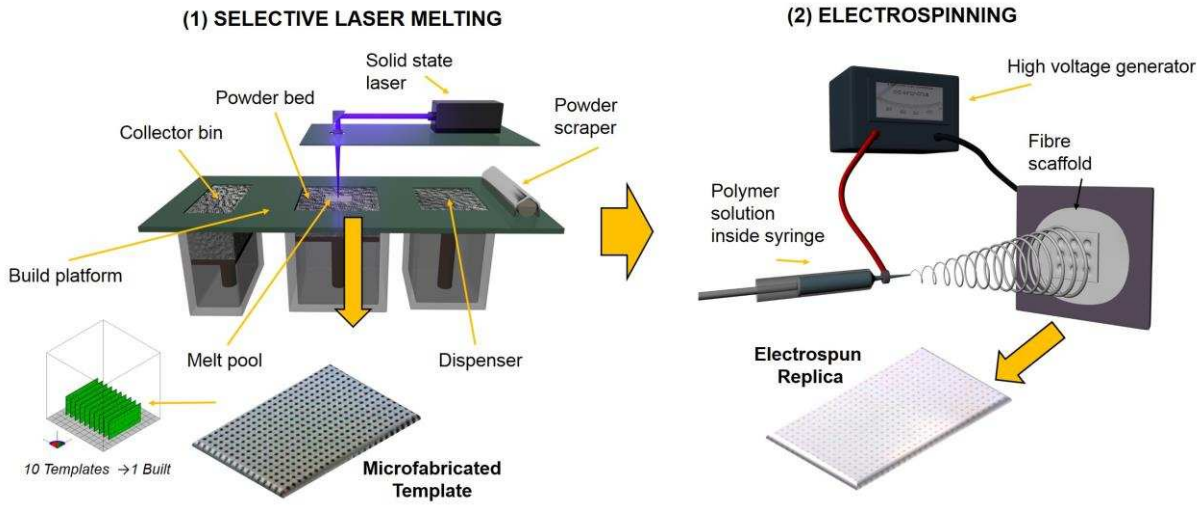

Figure 1. Schematic of the manufacturing process comprising two parts: (1) the use of SLM for manufacturing the stainless steel templates with a variety of niche-like topographies (fitting 10 templates in a single built) (1); the use of electrospinning for creating a biodegradable complex electrospun replica with controlled topography (2).

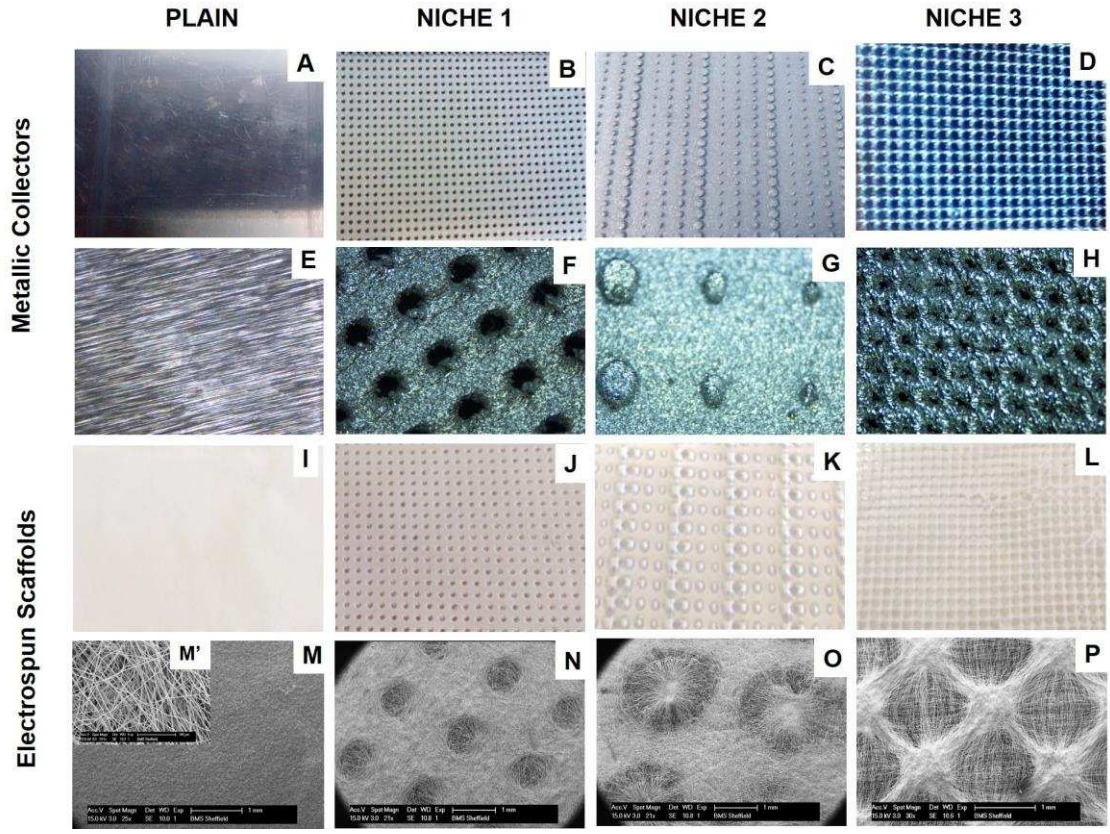

Figure 2. Optical and scanning electron microscopy micrographs of SLM-manufactured metallic collectors and electrospun scaffolds. Images A-D show a plain collector and three of the chosen niche-morphologies (x1 magnification); Images E-H are higher resolution optical

micrographs showing the metallic structures (x5 magnification); Images I-L show plain and niche- electrospun mats (x1 magnification); Images M-P are SEM micrographs of the plain electrospun scaffold and the three selected niche morphologies, scale bar is 1 mm.

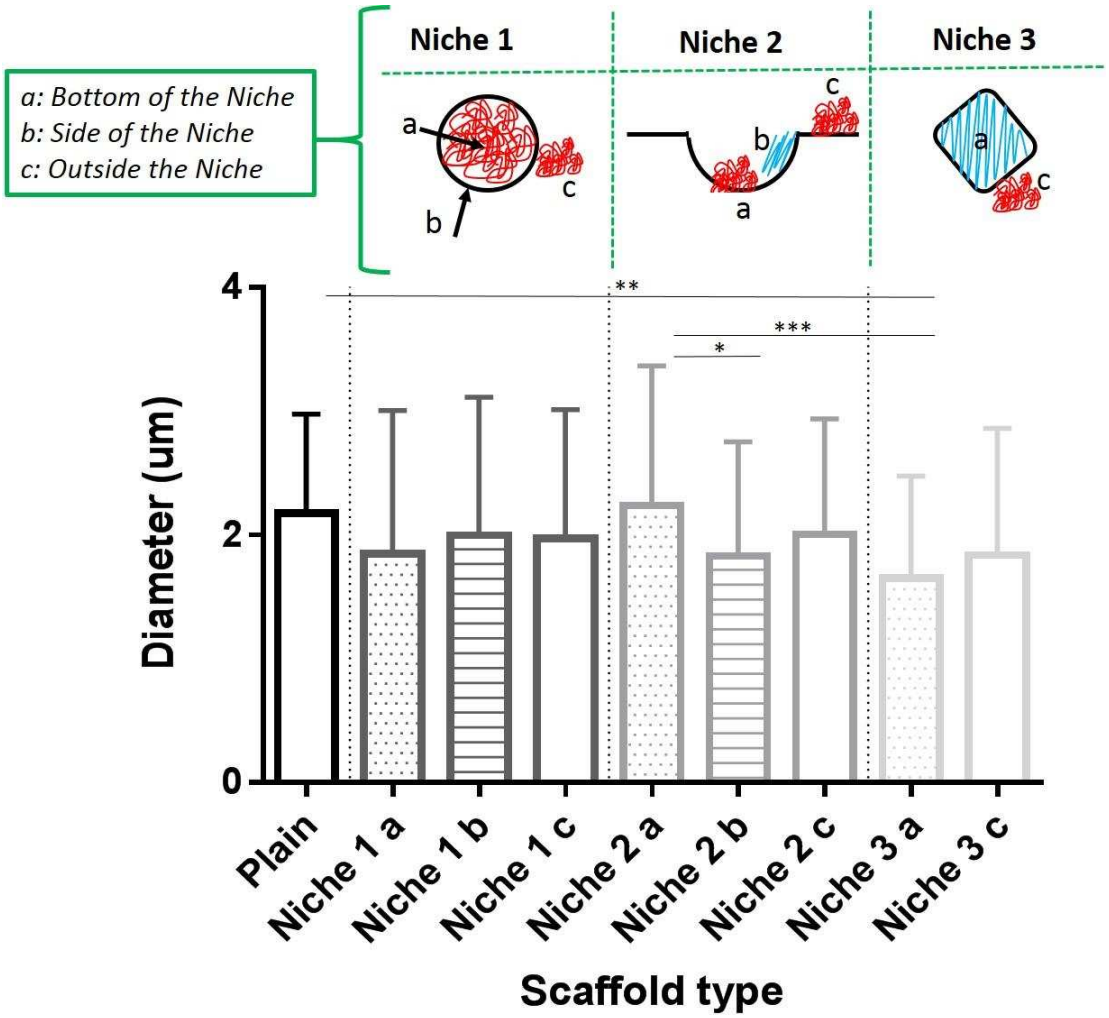

Figure 3. Plot highlighting the differences in fibre diameter between plain scaffolds and Niche 1, Niche 2 and Niche 3, and schematic highlighting the different areas of the Niche structures chosen for measuring fibre diameter ("a", inside the niche; "b", lateral or side of the niche; "c", outside the niche).

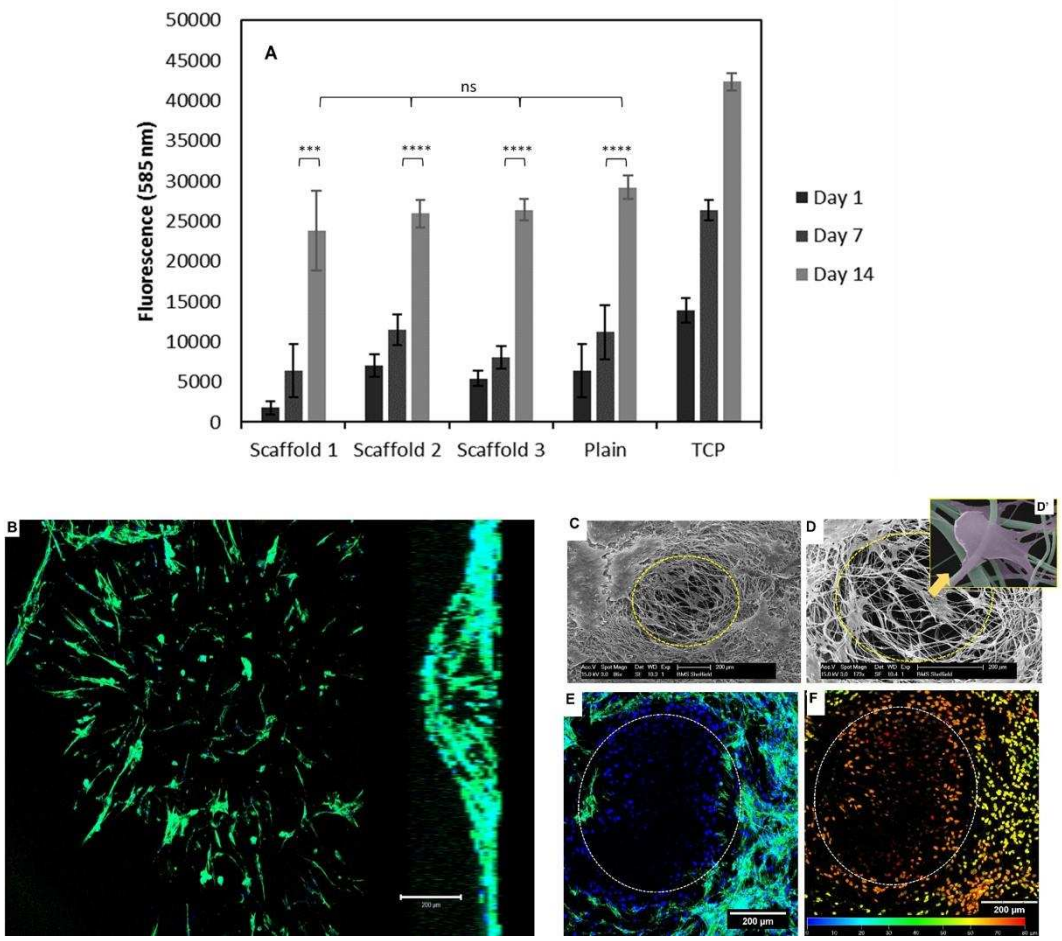

Figure 4. PrestoBlue values (emission at 635nm) at 1, 7 and 14 days showing the proliferation of MSC cells both in plain scaffolds and niche morphologies; the samples were compared to a TCP-2D control. No significant differences were observed between the plain scaffold and the scaffolds containing microfeatures (A); confocal z-stack of Phalloidin-FITC stained (green) rat MSCs on a scaffold 2 Niche-like structure (x10 magnification) (B); SEM image of a type1 Niche-like structure supporting MSC cell growth within the microenvironment area and in its surroundings (scale bar is 200 µm) (C, D); D' is showing an SEM false coloured micrograph of an MSC cell inside the niche microenvironment; Confocal image of a scaffold 2 niche presenting MSC growth (phalloidin-FITC (green) and DAPI (blue)) within and outside the microenvironment (x10 magnification) (E); Confocal representation highlighting the differences of depth within a microenvironment type 1 and its surroundings showing a map of cell nuclei distribution (F).

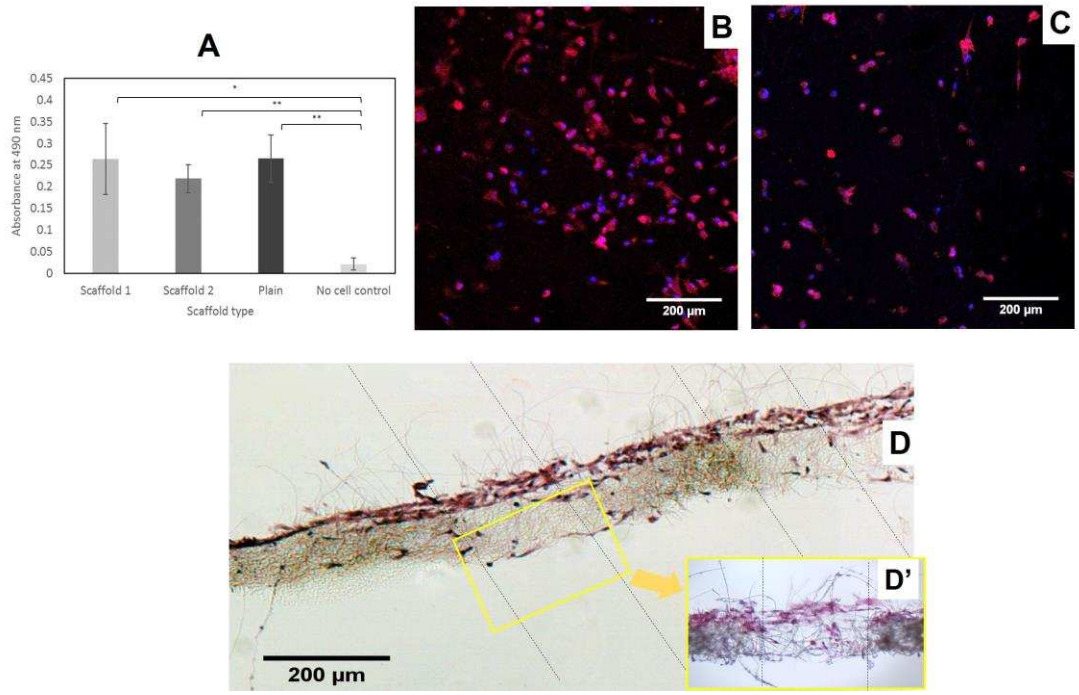

Figure 5. Sirius red measurements showing collagen deposition in samples with niches and plain scaffolds. A plain scaffold was used as a control. No significant differences were observed between scaffolds with and without niches (A). Confocal image of DAPI and CD44 on a plain scaffold after 7 days in culture (x10 magnification) (B). Confocal image of DAPI and CD44 on a type 1 scaffold after 7 days in culture (C). H&E stain of a 10 µm thick section of a scaffold (x5 magnification)(D). H&E optical image of a 10 µm thick section of a scaffold displaying the inter-niche area (x20 magnification) (D').

References

1. **Melchels, F.P.W., et al., *Additive manufacturing of tissues and organs.* Progress in Polymer Science, 2012. 37(8): p. 1079-1104.**
2. **Giannitelli, S.M., et al., *Current trends in the design of scaffolds for computer-aided tissue engineering.* Acta Biomaterialia, 2014. 10(2): p. 580-594.**
3. **Marga, F., et al., *Toward engineering functional organ modules by additive manufacturing.* Biofabrication, 2012. 4(2): p. 022001.**
4. **Huang, S.H., et al., *Additive manufacturing and its societal impact: a literature review.* The International Journal of Advanced Manufacturing Technology, 2013. 67(5): p. 1191-1203.**
5. **Narayan, R.J., et al., *Medical prototyping using two photon polymerization.* Materials Today, 2010. 13(12): p. 42-48.**
6. **Melchels, F.P.W., J. Feijen, and D.W. Grijpma, *A review on stereolithography and its applications in biomedical engineering.* Biomaterials, 2010. 31(24): p. 6121-6130.**
7. **Koutsoukis, T., et al., *Selective Laser Melting Technique of Co-Cr Dental Alloys: A Review of Structure and Properties and Comparative Analysis with Other Available Techniques.* J Prosthodont, 2015. 24(4): p. 303-12.**
8. **Sun, Z., et al., *Selective laser melting of stainless steel 316L with low porosity and high build rates.* Materials & Design.**

9. Korpela, J., et al., *Biodegradable and bioactive porous scaffold structures prepared using fused deposition modeling.* J Biomed Mater Res B Appl Biomater, 2013. 101(4): p. 610-9.
10. McCullough, E.J. and V.K. Yadavalli, *Surface modification of fused deposition modeling ABS to enable rapid prototyping of biomedical microdevices.* Journal of Materials Processing Technology, 2013. 213(6): p. 947-954.
11. Claeyssens, F., et al., *Producing electrospun scaffold used as medicament in e. g. corneal replacement involves electrospinning polymer or co-polymer onto template comprising conductive collector having three dimensional pattern to deposit the electrospun polymer*, in *Patent Number: US2015118197-A1* U. SHEFFIELD(USFF-C), Editor.
12. Ortega, I., et al., *Combination of Microstereolithography and Electrospinning to Produce Membranes Equipped with Niches for Corneal Regeneration.* JoVE, 2014(91): p. e51826.
13. Ortega, I., et al., *Combined microfabrication and electrospinning to produce 3-D architectures for corneal repair.* Acta Biomater, 2013. 9(3): p. 5511-20.
14. Ortega, I., et al., *Characterisation and evaluation of the impact of microfabricated pockets on the performance of limbal epithelial stem cells in biodegradable PLGA membranes for corneal regeneration.* Biomaterials Science, 2014. 2(5): p. 723-734.
15. Raimondi, M.T., et al., *Three-dimensional structural niches engineered via two-photon laser polymerization promote stem cell homing.* Acta Biomaterialia, 2013. 9(1): p. 4579-4584.
16. Gill, A., et al., *Towards the fabrication of artificial 3D microdevices for neural cell networks.* Biomedical Microdevices, 2015. 17(2): p. 1-10.
17. Ortega, I., et al., *Development of a microfabricated artificial limbus with micropockets for cell delivery to the cornea.* Biofabrication, 2013. 5(2): p. 1758-5082.
18. Yoon, J.K., et al., *Enhanced Bone Repair by Guided Osteoblast Recruitment Using Topographically Defined Implant.* Tissue Eng Part A, 2016. 22(7-8): p. 654-64.
19. Müller, E., et al., *Space constraints govern fate of hematopoietic stem and progenitor cells in vitro.* Biomaterials, 2015. 53(0): p. 709-715.
20. Moeller, H.-C., et al., *A microwell array system for stem cell culture.* Biomaterials, 2008. 29(6): p. 752-763.
21. Levis, H.J., et al., *Rapid tissue engineering of biomimetic human corneal limbal crypts with 3D niche architecture.* Biomaterials, 2013. 34(35): p. 8860-8868.
22. Truckenmüller, R., et al., *Fabrication of cell container arrays with overlaid surface topographies.* Biomedical Microdevices, 2012. 14(1): p. 95-107.
23. Fuchs, E., T. Tumbar, and G. Guasch, *Socializing with the Neighbors: Stem Cells and Their Niche.* Cell, 2004. 116(6): p. 769-778.
24. Lutolf, M.P., P.M. Gilbert, and H.M. Blau, *Designing materials to direct stem-cell fate.* Nature, 2009. 462(7272): p. 433-441.
25. Lutolf, M.P. and H.M. Blau, *Artificial Stem Cell Niches.* Advanced Materials, 2009. 21(32-33): p. 3255-3268.
26. Xu, D., N. Xiang, and B. Wei, *The marginal fit of selective laser melting-fabricated metal crowns: an in vitro study.* Journal of Prosthetic Dentistry, 2014. 112(6): p. 1437-1440.
27. Santocildes-Romero, M.E., et al., *Preparation of Composite Electrospun Membranes Containing Strontium-Substituted Bioactive Glasses for Bone Tissue Regeneration.* Macromolecular Materials and Engineering, 2016.
28. Maniatopoulos, C., J. Sodek, and A.H. Melcher, *Bone formation in vitro by stromal cells obtained from bone marrow of young adult rats.* Cell Tissue Res, 1988. 254(2): p. 317-30.
29. Kaukua, N., et al., *Glial origin of mesenchymal stem cells in a tooth model system.* Nature, 2014. 513(7519): p. 551-+.
30. Fisher, O.Z., et al., *Bioinspired Materials for Controlling Stem Cell Fate.* Accounts of Chemical Research, 2010. 43(3): p. 419-428.

31. **Gnavi, S., et al., *The influence of electrospun fibre size on Schwann cell behaviour and axonal outgrowth.* Materials Science and Engineering: C, 2015. 48: p. 620-631.**
32. **Qu, J., et al., *Optimization of electrospun TSF nanofiber alignment and diameter to promote growth and migration of mesenchymal stem cells.* Applied Surface Science, 2012. 261: p. 320-326.**
33. **Edmondson, R., et al., *Three-dimensional cell culture systems and their applications in drug discovery and cell-based biosensors.* Assay Drug Dev Technol, 2014. 12(4): p. 207-18.**
34. **Zoller, M., *CD44: can a cancer-initiating cell profit from an abundantly expressed molecule?* Nat Rev Cancer, 2011. 11(4): p. 254-67.**
35. **Dominici, M., et al., *Minimal criteria for defining multipotent mesenchymal stromal cells. The International Society for Cellular Therapy position statement.* Cytotherapy, 2006. 8(4): p. 315-317.**
36. **Boxall, S.A. and E. Jones, *Markers for characterization of bone marrow multipotential stromal cells.* Stem Cells Int, 2012. 2012: p. 975871.**
37. **Barzilay, R., et al., *Comparative characterization of bone marrow-derived mesenchymal stromal cells from four different rat strains.* Cytotherapy, 2009. 11(4): p. 435-42.**
38. **Braam, S.R., et al., *Recombinant vitronectin is a functionally defined substrate that supports human embryonic stem cell self-renewal via alphavbeta5 integrin.* Stem cells (Dayton, Ohio), 2008. 26(9): p. 2257-2265.**
39. **Mei, Y., et al., *Combinatorial development of biomaterials for clonal growth of human pluripotent stem cells.* Nat Mater, 2010. 9(9): p. 768-778.**